On the Resistances of a Slurry Electrode Vanadium Redox Flow Battery

Korcan Percin,[a, b] Bart van der Zee,[c] and Matthias Wessling*[a, b]

We studied the half-cell performance of a slurry-based vanadium redox flow battery via the polarization and electrochemical impedance spectroscopy methods. First, the conductive static mixers are examined and lower ohmic and diffusion resistances are shown. Further analyses of the slurry electrodes for the catholyte (VO^{2+}–VO_2^+) and anolyte (V^{3+}–V^{2+}) are presented for the graphite powder slurry containing up to 15.0 wt.% particle content. Overall, the anolyte persists as the more resistive half-cell, while ohmic and diffusion-related limitations are the dominating resistances for both electrolytes. The battery is further improved by the addition of Ketjen black nanoparticles, which results in lower cell resistances. The best results are achieved when 0.5 wt.% Ketjen black nanoparticles are dispersed with graphite powder since the addition of nanoparticles reduces ohmic, charge transfer and mass diffusion resistances by improving particle-particle dynamics. The results prove the importance of understanding resistances in a slurry electrode system.

1. Introduction

The interest in electrical energy storage systems for the grid is growing steadily due to supply fluctuations caused by the integration of renewable energy sources.[1] Large-scale energy storage systems are necessary as a buffer between energy production and grid consumption for applications like peak shaving and load leveling.[2] One of the most promising technologies is redox flow batteries (RFBs), which enable a broad range of energy storage capacity with variable power outputs.[3,4] RFBs are advantageous as they decouple power and energy capacities. Most RFB technologies have electrolyte-based redox reactions, meaning that the electrodes are not consumed during battery operation. This enables the power to be controlled by the volume of the cell and the amount of stored energy to be controlled by the electrolyte volume stored in the external tanks.

One of the most researched RFBs is the vanadium redox flow battery (VRB).[5–9]. VRBs use vanadium as redox-active species, where redox reactions of VO^{2+}–VO_2^+ as catholyte and V^{3+}–V^{2+} as anolyte happen simultaneously. Solid porous electrodes, such as carbon felts or papers, are widely used in these batteries.[10–12] The electrodes do not contribute to the redox reactions, except for the fact that they provide sufficient surface area for electrolyte reactions, leading to higher current densities. Recently, a novel approach has been introduced that renders the traditional concept of static solid porous electrodes to a more dynamic level.[13] In this approach, conductive particle networks, called slurry electrodes, are used to transport the electrons to the electrolyte.

Slurry electrodes are conductive particles dispersed in an electrolyte. The dispersion of the particles is recirculated with the electrolyte in an electrochemical flow cell. The particles form a continuous charge transfer mechanism via inherently induced particle-particle and particle-current collector contacts. When the conductive particle bridge is maintained, either the storage of the charge in the particle or the direct transfer of the charge to the redox-active species can be achieved. Several applications are already available in the literature: flow capacitive deionization,[14] electrochemical flow capacitor,[15] and redox flow battery.[16] A system with slurry electrodes benefits from: (1) high surface area of the particles; (2) ease of production; (3) scalability of the electrode surface area independently from the cell volume; (4) maintenance through particle recycling.

Carbon particles are usually the material of choice for the slurry electrodes in different applications [16–18]. Particle properties such as size, shape, electrical conductivity, and porosity play a critical role in the charge transfer for each application. A specific volume ratio of particle-to-electrolyte is required to enable the highest charge transfer. This phenomenon has already been described with the particle percolation theory that predicts better charge transfer with higher particle content.[15,19] However, more pumping power is required as viscosity increases with higher particle-to-electrolyte ratio; therefore, detailed analyses of the particle properties and the rheology of the suspension are necessary to find the best performing suspension.[20]

[a] K. Percin, Prof. Dr.-Ing. M. Wessling
DWI-Leibniz Institute for Interactive Materials
Forckenbeckstr. 50, 52074 Aachen, Germany
[b] K. Percin, Prof. Dr.-Ing. M. Wessling
RWTH Aachen University,
Aachener Verfahrenstechnik-Chemical Process Engineering
Forckenbeckstr. 51, 52074 Aachen, Germany
Fax: (+49) 24180–92252
E-mail: manuscripts.cvt@avt.rwth-aachen.de
[c] B. van der Zee
KU Leuven, Department of Chemical Engineering
Oude Markt 13, 3000 Leuven, Belgium

© 2020 The Authors. Published by Wiley-VCH Verlag GmbH & Co. KGaA. This is an open access article under the terms of the Creative Commons Attribution Non-Commercial NoDerivs License, which permits use and distribution in any medium, provided the original work is properly cited, the use is non-commercial and no modifications or adaptations are made.

One of the main challenges is that the slurry electrodes are shear-thinning fluids. Therefore, the flow profile under laminar conditions will suffer from stagnant flow rates in proximity to the electrode surface (Figure 1). On the contrary, slurry particles require more turbulent flow regimes, which force particles to mix and increase the contact between particles and the current collector. A simple approach to increasing the turbulent flow is using static mixers in membrane separation and electrochemical processes.[21–23] Static mixers are flow promoters that induce additional secondary flows to the flow field; therefore, they help to mitigate the mass transport related limitations. As recently shown by our group, static mixers improve the particle movements in the flow cell and enable the slurry electrodes to reach higher polarization current densities.[13] To have a better understanding of resistances that limit the performance, slurry electrodes should be studied thoroughly in a VRB.

In this work, we further investigate the utilization of slurry electrodes and thereby elucidate the half-cell resistances in a VRB. Polarization and electrochemical impedance spectroscopy (EIS) measurements are used to evaluate overpotentials and resistances resulting from ohmic, charge transfer and diffusion processes during charge and discharge. Subsequently, a particle additive is introduced to increase the performance of the slurry electrodes by improving the electrical conductivity, thus reducing the overpotentials and their resistances.

Experimental Section

Electrolyte Preparation

Commercial vanadium electrolyte was purchased as a mixture of total 1.6 M $VOSO_4/V_2(SO_4)_3$ in 4 M sulfuric and phosphoric acid media (GfE Metalle und Materialien GmbH, Germany). The experiments were all done at 50% state of charge (SOC). For this, the electrolyte was charged in a VRB using standard graphite felts (GFD4.6 EA, SGL Group, Germany).

Slurry electrodes were prepared by manually adding conductive particle powders to the solutions on a mass fraction base. Synthetic graphite powder (GP) (Sigma-Aldrich Co., Germany) with an average size below 20 μm was used as the main slurry particle and Ketjen black® (KB) EC600-JD (Fitz Chem LLC, USA), a type of carbon black, with an average size of 34 nm was used as the additive particle. The weight fractions of the slurries were set to 0.0, 5.0, 7.5, 10.0, and 15.0 wt.%. The KB percentage was established as 0.5 and 1.0 wt.%, while the total weight fraction of the particles was kept constant at 15.0 wt.%. Slurry electrodes containing KB were then mixed for at least half an hour with magnetic stirrers. The electrolyte flow was maintained at 20 mL/min with a peristaltic pump (Masterflex L/S, Cole Parmer). The volume of the both positive and negative electrolytes were kept at 50 mL.

Cell

A laboratory sized flow cell was used with an effective area of 19 cm^2 as described in our previous paper.[13] The static mixers (SM) were produced via additive manufacturing with a single layer of twisted filaments (Stratasys Objet Eden 260 V, RGD525). The SMs were etched in 75% sulfuric acid for 10 minutes and then spray coated with conductive graphite lacquer (Graphit, Cramolin). The conductive layer was applied to assure a better charge transfer from the current collectors to the particles. Thereby, the active surface area is increased where the charge is delivered to/from the slurry electrodes while the flow distribution is maintained by the static mixers.

Electrochemical Measurements

A potentiostat/galvanostat with an integrated impedance module (PGSTAT302 N, Metrohm GmbH) was used for all measurements and overpotentials were measured with multimeters (PeakTech 2025). The experimental setup for overpotential measurements is illustrated in Figure 2a. Half-cell overpotentials were resolved via external voltage measurements. Therefore, PVC connectors were placed as measurement cells for both electrolyte. A glassy carbon electrode (PalmSens BV, The Netherlands) and a $Hg/HgSO_4$ reference electrode filled with 0.5 M sulfuric acid (Xylem Analytics GmbH., Germany) were inserted in the measurement cells and used for overpotential and half-cell potential evaluations. The surface area for the current density was defined from the active surface area of the graphite plates. Constant current steps of 5 $mA\,cm^{-2}$ were applied alternately between charging and discharging. The currents were applied for 30s and the resulting cell potential values were recorded. The open circuit potential (OCP) was kept in a constant range of ±20 mV before every new measurement. The

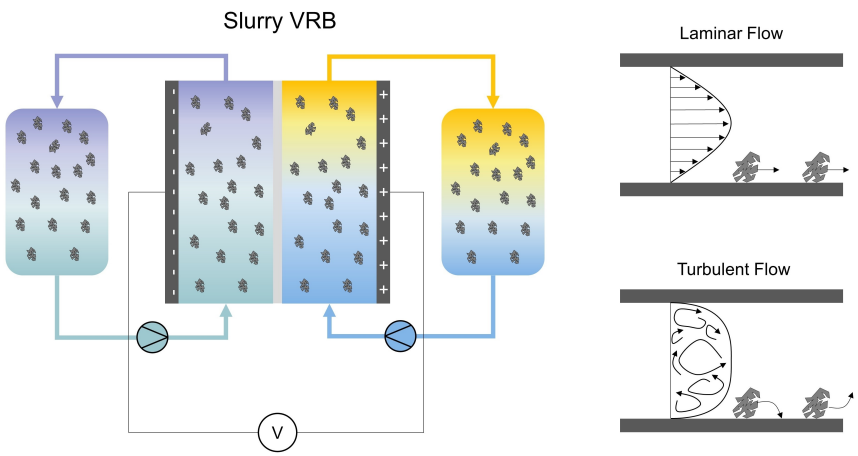

Figure 1. A slurry vanadium redox flow battery (left) and particle flow profiles for laminar and turbulent flow (right).

© 2020 The Authors. Published by Wiley-VCH Verlag GmbH & Co. KGaA

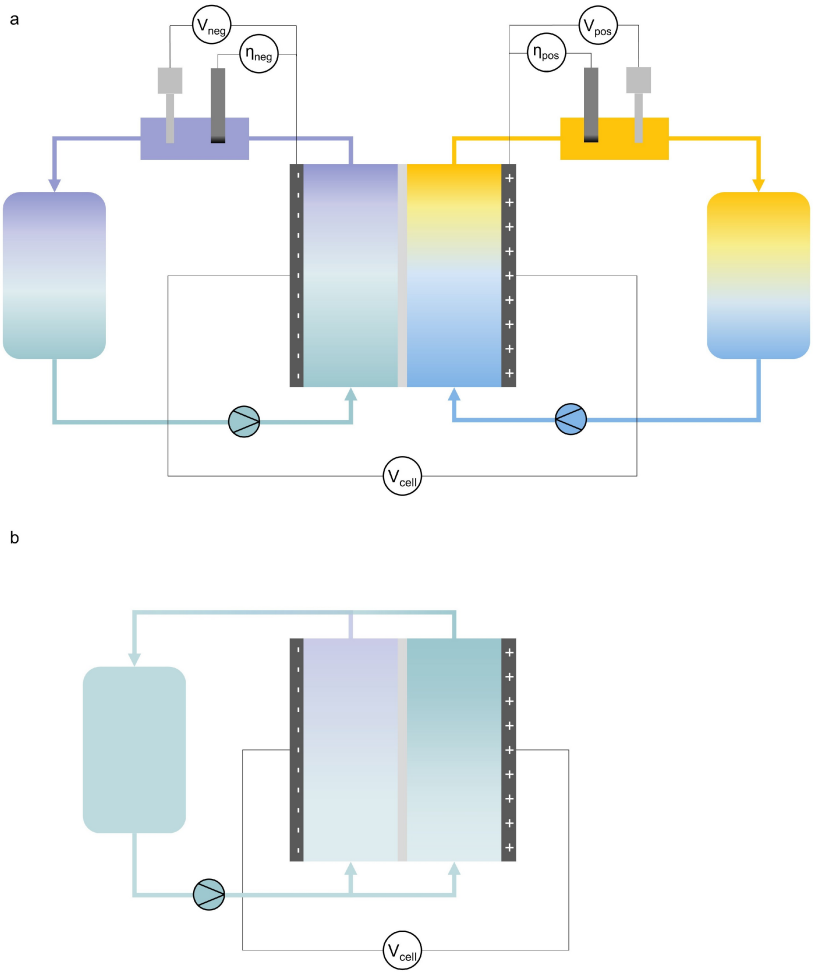

Figure 2. Schematic showing the experimental setup used for a) polarization measurements, b) electrochemical impedance spectroscopy with symmetric electrolyte flow (single electrolyte flowing through both half cells).

polarization experiments were done until the charge potential of 1.85 V, and discharge potential of 0.8 V were reached.

EIS experiments were performed with a symmetrical cell setup as shown in Figure 2b. Only one electrolyte was circulated through both sides of the cell, by connecting the outlet of one chamber to the inlet of the other. The electrolyte is fed to a flow dampener right after the peristaltic pump to reduce fluid pulsations, which may have an effect on the impedance results. Settling of the particles in the dampener was prevented with a magnetic stirrer. An alternating potential signal with an RMS amplitude of 5 mV was applied. The frequency of the signal is measured from 30 kHz to 0.1 Hz. Direct potential during the EIS experiments was set to 0.1 V over the OCP values. No negative potentials were used, because the symmetric electrolyte flow provides similar results. Between each measurements, a waiting time of 30 s was applied to let the particles reach a steady state of OCP. The EIS data was handled and further modelled in ZView® (Scribner) software.

2. Results and Discussion

All the EIS data are modelled using the equivalent circuit shown in Figure 3a. The equivalent circuit of the model is adapted from Rommerskirchen et al., which describes an EIS methodology for a flow capacitive deionization (FCDI) process using porous activated carbon particles as slurry electrodes.[24] The resistances that accumulate in a FCDI module resemble highly those of a VRB that utilizes slurry electrodes. The difference between the two processes is that the FCDI process does not engage faradaic reactions, while the VRB exclusively focuses on the faradaic reactions of redox species. On the other hand, due to extremely high porosity of activated carbon in the FCDI process, the convective properties become critical. Since we could not determine a difference between modelling with or without convective resistances, they are neglected in this study.

The ohmic resistances (R_{ohm}) are defined at the high frequency region (1000 Hz $< \omega$) modelled with a resistor. R_{ohm} includes contact resistances between electrolyte and electrodes, electrolyte resistances, and membrane resistance in the cell. The middle range frequencies (10 Hz $< \omega <$ 1000 Hz) characterize mostly the charge transfer resistances (R_{ct}). A resistor, R_{ct}, depicts both faradaic reactions near the current collector and the charge transfer resistance of the particles that make contact with the surface. Here, the traditional parallel capacitor is exchanged with a constant phase element (CPE_{ct}), as the

© 2020 The Authors. Published by Wiley-VCH Verlag GmbH & Co. KGaA

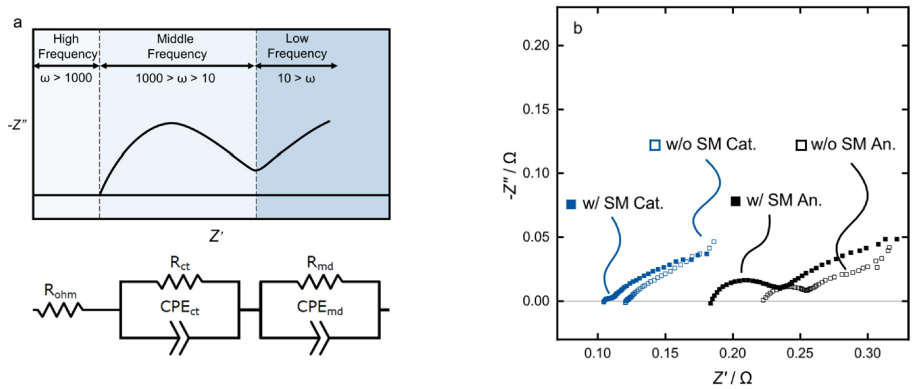

Figure 3. a) EIS frequency spectrum (top) with the modified[24] equivalent circuit model (bottom), b) Comparison of static mixer usage (with SM (■) and without SM (□)) for catholyte (blue) and anolyte (black) with 15.0 wt.% slurry electrodes via EIS.

capacitance of the current collector surface and the particles itself are constantly disturbed by the redox reactions, causing imperfect capacitor behavior. Towards the low frequency region ($\omega < 10$ Hz) mass diffusion related resistances (R_{md}) are slightly prominent giving the Nyquist plot a slightly flat zone.[18] Very low frequencies are highly sensitive to pulsating electrolyte flow caused by pumps. A flow dampener is used to eliminate some of the oscillations. Yet, some disturbance can be observed at very low frequencies before the second semi-circle of the Nyquist plots is complete. Therefore, we decided to stop the measurements right before the oscillations ($\omega = 0.1$ Hz).

2.1. Effects of Static Mixers on Cell Resistances

The benefit of using SMs has been shown previously through only full cell polarization experiments.[13] For that reason, EIS experiments are conducted to evaluate the improvements on the cell resistances, and analyzed for each anolyte (V^{3+}–V^{2+}) and catholyte (VO^{2+}–VO_2^+). The Nyquist plots are presented in Figure 3b. The anolyte shows overall higher resistances as the catholyte, which is in correlation with previous published research.[13] A direct observation can be made through checking R_{ohm} where the Nyquist plots intersects with y-axis ($y = 0$). Using SMs drastically reduce the ohmic resistances for each catholyte and anolyte. With the help of better mixing in the flow field, the concentration polarization is reduced, resulting in higher ionic conductivity.[22,25] Similar behavior can be calculated for R_{md} from the modelling results, where using SMs lowers the mass diffusion resistances from 0.29 to 0.10 Ω at the catholyte and 0.27 to 0.14 Ω at the anolyte. The improvement of the ion transport can also be explained by better mixing in the flow field. A clear increase of R_{ct} can be seen from the length of the first semicircles. R_{ct} is four times higher when SMs are used for catholyte and two times higher for anolyte. We can explain the increase of charge resistances by the high surface roughness of the SMs. The conductive graphite coating on the SMs creates surface roughness, on which micron-sized particles may easily be attached. This prolongs the charge transfer pathway and thus, higher charge transfer resistances occur. Nevertheless, as the results of our previous polarization experiments with 15.0 wt.% graphite powder and SM show improved polarization behavior, we can conclude that R_{ohm} and R_{md} have a higher impact than R_{ct} for the battery application.[13]

2.2. Half-Cell Overpotential and Resistances

The primary goal in this study is to resolve the overpotentials in each half cell, and identify the main contributing resistances. Firstly, full cell experiments are done at 50% SOC and the performance of the overall battery among different slurry concentrations are evaluated. Approximately 1.4 V OCP is set as the constant before each measurement point. Figure 4a depicts the resulting polarization curves. The cell potential is corrected for ohmic resistances, which is measured by full cell EIS measurement. The highest particle concentration is set to 15.0 wt.% to avoid clogging issues. Both charge and discharge polarization curves show positive correlation to the increased particle concentration by having higher current densities for higher content of slurry electrodes. The charge -2 side of the polarization (positive current densities) reaches 70mAcm current density with 15.0 wt.% slurry electrodes, as does the discharge side (negative current densities). Compared to our previous study, we can distinguish a slight difference between polarization at 0%-100% SOC for charge and discharge and polarization at 50% SOC.[13] The half-charged state of the electrolytes shows more realistic resistance values, as the losses caused by activation and mass transport are equally effective. Therefore, maximum current densities that can be achieved by this study show slightly lower results.

Half-cell contributions on the 15.0 wt.% slurry electrodes are shown in Figure 4b. The catholyte and anolyte overpotentials are relatively similar being approximately 30 mV for both charge and discharge. The highest contribution to the total overpotential is the ohmic overpotential (η_{ohm}) with up to 180 mV at 70 mA cm^{-2}. It is therefore obvious that the ohmic resistances that persist when using slurry electrodes are one of the limiting factors in the system.

© 2020 The Authors. Published by Wiley-VCH Verlag GmbH & Co. KGaA

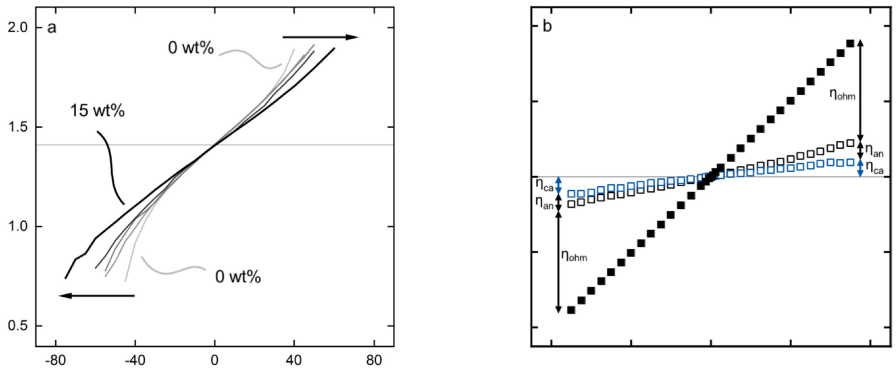

Figure 4. a) Full cell polarization of slurry electrodes from 0 to 15 wt.%, b) catholyte (η_{ca}), anolyte (η_{an}), and ohmic (η_{ohm}) overpotentials of 15 wt.% slurry electrodes.

The breakdown of the half-cell resistances with EIS is presented in Figure 5. The single electrolyte system evaluates catholyte and anolyte separately, therefore more distinctive analysis of the resistances can be made. The Nyquist plots of the catholyte with increasing particle content are presented in Figure 5a and the resolved resistances in Figure 5b. Ohmic resistances show a slight increase with higher particle content. R_{ohm} increases from 0.09 to 0.11 Ω for the catholyte. Due to the higher content of non-ionic slurry particles, the ionic transport pathway in the electrolyte is partially blocked, causing this slight increase in the ohmic resistance. A decrease in the charge transfer resistances can be seen, with it having the lowest resistance values among all. R_{ct} decreases from 0.010 to 0.007 Ω with higher particle content. Meaning that the more particles the slurry electrodes have, the better the charge transfer is. The final and the highest resistance is the mass diffusion resistance. Surprisingly, R_{md} decreases from 0.25 to 0.20 Ω. A swift decrease of R_{md} occurs between 5 and 7.5 wt.% slurry, where presumably particle-particle interactions become observable. Particle percolation theory describes a critical ratio of particle content for the dispersion to form highly conductive particle percolations.[19,26,27] Although it has been suggested that better charge transfer may be obtained with particle percolations, however, the low values of R_{ct} do not reveal an apparent proof for better charge

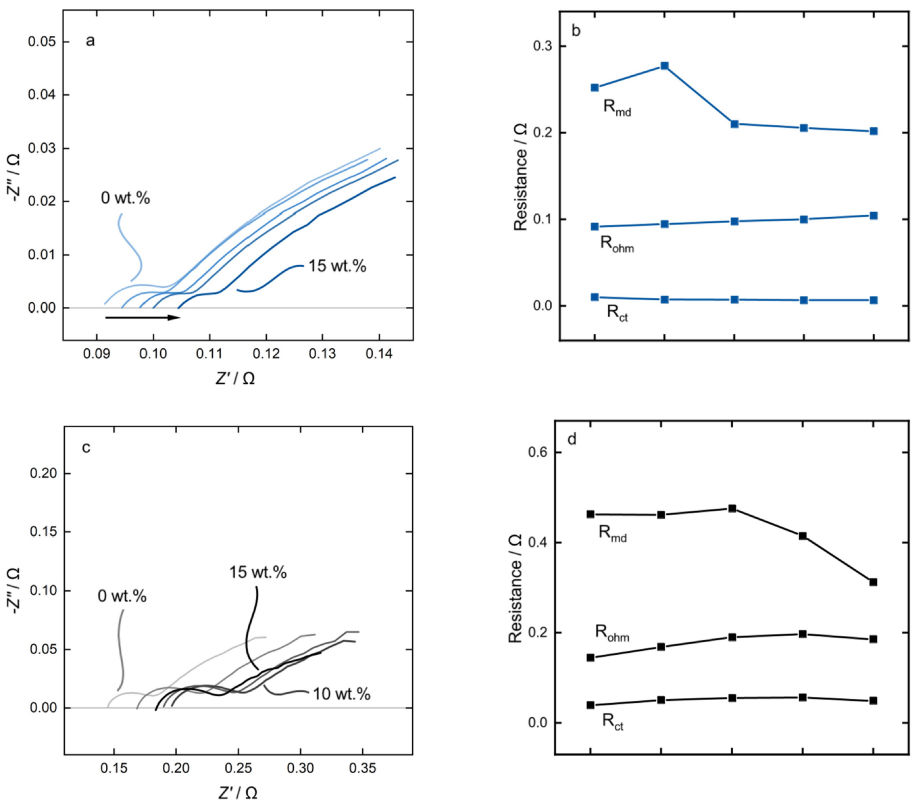

Figure 5. Half-cell resistances; a) the Nyquist plot for the catholyte, b) resolved resistances for the catholyte, c) the Nyquist plot for the anolyte, d) resolved resistances for the anolyte, mass diffusion presented with R_{md}, ohmic with R_{ohm}, and charge transfer with R_{ct}.

© 2020 The Authors. Published by Wiley-VCH Verlag GmbH & Co. KGaA

transfer phenomena. The improvement of R_{md} is more distinct in this case and further improvements should be considered for further reduction.

We investigate further on the anolyte resistances in Figure 5c–d. Similar to the catholyte, anolyte ohmic resistance shows an increase with the higher particle content. Only the slurry electrodes with 15.0 wt.% showed a decrease at the R_{ohm} right after the 10.0 wt.% slurry electrodes. As the ohmic resistance is measured in the high frequency region, the EIS measurement is highly responsive to the minimal changes, such as constantly occurring particle percolations. The decrease at the ohmic resistance is possibly due to the instantaneous change in the flow profile of the electrolyte. However, comparing to the overall resistances in the Figure 5d, it does not lead to any noticeable consequence. Total increase of R_{ohm} is from 0.14 to 0.19 Ω. It is worth noticing that anolyte ohmic resistances are almost twice as high as the catholyte ohmic resistances. The charge transfer resistances in anolyte demonstrates a slight increase from 0.04 to 0.05 Ω, which conflicts with the behavior of R_{ct} for the catholyte. Nevertheless, the charge transfer resistances of the anolyte are higher compared to the catholyte. Finally, R_{md} is again the highest resistance for the anolyte, beginning at 0.46 Ω and decreasing to 0.31 Ω with higher particle content. The decrease starts after the 10.0 wt.% slurry content, which verifies the previous findings on the catholyte, namely that the particle percolation threshold has a distinct impact on mass transport resistances. Overall all the anolyte resistances that are presented, show higher values than the catholyte, which is the same relation as is shown in the literature.[28]

2.3. Improving Resistances by Ketjen Black

According to our results obtained from full cell and half-cell polarization and EIS studies, the main limitations of the slurry electrodes are due to the ohmic and the diffusion related resistances in the VRB. Therefore, reducing these resistances would be beneficial for the applicability of slurry based systems. GP used in the slurry electrodes are micro sized (< 20 μm) and sharply shaped. Electrical conductivity depends on the contact area between these particles, which is mainly limited by the shape. One possible approach is to use a conductive additive within the slurry electrodes to increase the conductivity.[29,30] In this work, we used KB nanoparticles as conductive additive for the GP slurries. The conductivity of the particle network is improved by the nanoparticles filling the GP-GP voids, thus creating higher surface area for the charge transfer.

The use of KB with GP slurry electrodes is illustrated in Figure 6a. KB addition to the GP slurry electrode is done by 0.5 and 1.0 wt.%, respectively. The total weight percentage is kept constant at 15.0 wt.% slurry electrode. The addition of KB could not be increased further, as the viscosity of the slurry electrodes become inapplicable. Figure 6b shows the full cell polarization of the 15.0 wt.% GP, 14.5 wt.% GP + 0.5 wt.% KB, and 14.0 wt.% GP + 1.0 wt.% KB. Both KB added slurry electrodes perform better on the charge and discharge polarization by having higher current densities. Interestingly, 0.5 wt.% KB addition shows the best performance increasing the discharge current density from 65 to 80 mA cm^{-2} at a constant overpotential of approx. 340 mV. The same behavior can be seen on the charge side where the current density increase from 60 to 75 mA cm^{-2} at a constant overpotential of approx. 250 mV. At the same time, the 1.0 wt.% addition of KB results in slightly lower current densities than 0.5 wt.% on the discharge side, while the charge side is very similar to the results of 0.5 wt.% KB addition. This suggests that using small amounts of conductive additive can improve the slurry battery performance, but higher nanoparticle content may not have the best effect. This may be due to the excessive nanoparticle content that increases the viscosity of the slurry electrodes intensively and lowering the flow distribution quality in the flow cell.

Further EIS analysis is done to resolve the resistances that change with the addition of KB in each half cell. Figure 7a-b present the resistances for the catholyte and Figure 7c–d for the anolyte. R_{ohm} decreases from 0.11 to 0.09 Ω with 0.5 wt.% KB addition in the catholyte. A greater decrease in R_{ohm} can be observed at the anolyte side, R_{ohm} decreasing from 0.19 to 0.14 Ω with 0.5 wt.% KB addition. For both electrolytes, R_{ohm} with 1.0 wt.% KB addition shows lower resistances than only 15.0 wt.% GP but higher than 0.5 wt.% KB. The decrease in the ohmic resistances proves the hypothesis of the possible increase in the electrical conductivity by better particle-particle contact when the nanoparticles are used. The 1.0 wt.% KB addition however, increases the ohmic resistances again, which is due to presumably the dispersion quality that gets visibly

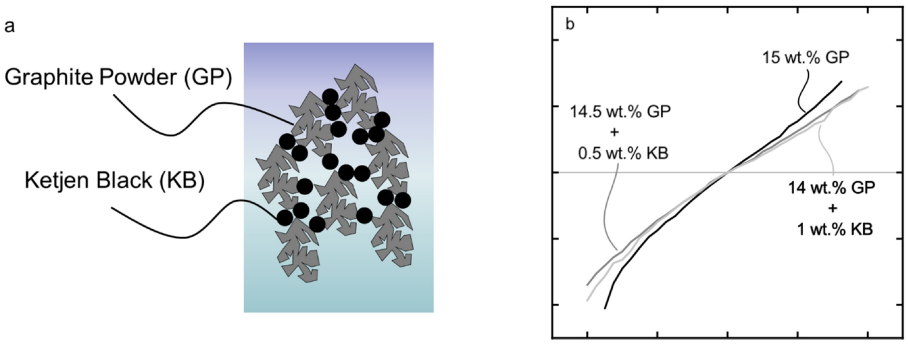

Figure 6. a) Illustration of KB addition to slurry electrodes, b) full cell polarization of the KB added slurry electrodes with total particle content of 15 wt.%.

© 2020 The Authors. Published by Wiley-VCH Verlag GmbH & Co. KGaA

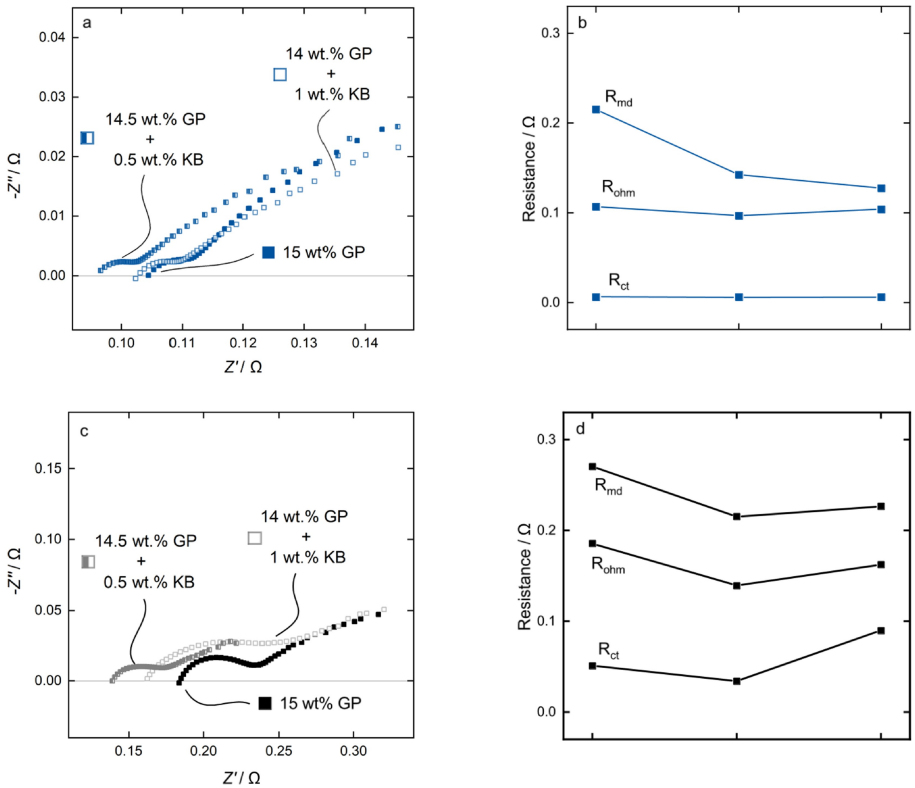

Figure 7. Half-cell resistances for the KB addition to the GP slurry electrodes; a) the Nyquist plot for the catholyte, b) resolved resistances for the catholyte, c) the Nyquist plot for the anolyte, d) resolved resistances for the anolyte.

worsened. The charge transfer resistances for catholyte and anolyte show similar trend. R_{ct} shows minimum resistance for 0.5 wt.% KB addition in both catholyte and anolyte with relatively low values. A noticeable difference is observed in the anolyte side for R_{ct}, by which the resistance increase is even higher than slurry electrodes without KB addition. Therefore, it is clear that a higher content of nanoparticles in the slurry electrodes has a negative effect on the charge transfer mechanism.

The highest improvement for the addition of the nanoparticles can be observed in the diffusion related resistances. R_{md} for the catholyte decreases from 0.22 to 0.13 Ω for 1.0 wt.% KB addition, surprisingly even lower than 0.5 wt.%. Nevertheless, the overall observation recurs for the anolyte, since the 0.5 wt.% KB addition shows the lowest R_{md}, which decreases from 0.27 to 0.23 Ω. We can explain the improved diffusion resistances by the disturbed particle percolations of the GP. Smaller KB particles constantly break the percolated GP particle network locally. Thus, local diffusion of the ions is highly improved. However, the overall recurrence of particle percolations becomes more frequent, leading to an enhancement of the ohmic and charge transfer resistances.

3. Conclusions

In this work, we further investigated the polarization behavior and limiting resistances for each half cell of a slurry electrode-based vanadium redox flow battery. Firstly, the effect of using static mixers was analyzed with the half-cell impedance measurements that indicate improved ohmic and mass transfer limitations when static mixers are utilized. Further analysis of each half cell showed a relatively high contribution of the ohmic and mass transfer resistances compared to charge transfer resistances. Higher particle content in the slurry electrodes improved the charge transfer and more explicitly the mass transfer resistances, whereas the ohmic resistances increased. Overall the catholyte half-cell of the battery showed less resistive behavior than the anolyte side in the slurry VRB.

After resolving and identifying the resistances for the slurry electrodes containing only graphite powder, nanosized Ketjen black particles were added to increase the conductivity and reduce the resistances in the battery. An addition of 0.5 and 1.0 wt.% Ketjen black was investigated in the graphite powder slurry with a total particle content of 15.0 wt.%. The best result was achieved with 0.5 wt.% Ketjen black addition which lowers the values of ohmic, charge transfer, and mass diffusion resistances. The effect of KB addition was demonstrated by the polarization study that shows the highest current densities with the 0.5 wt.% KB content, reaching 80 mA cm^{-2} when discharging. Ultimately, as a result of EIS and polarization studies, we can evaluate more on the nature of the slurry electrodes via analyzing and defining the resistances that exist and further improvement strategies can be established.

© 2020 The Authors. Published by Wiley-VCH Verlag GmbH & Co. KGaA

Acknowledgements

M.W. acknowledges the support of the Gottfried Wilhelm Leibniz award; This project has received funding from the European Research Council (ERC) under the grant agreement No. 694946.

Conflict of Interest

The authors declare no conflict of interest.

[1] B. Dunn, H. Kamath, J.-M. Tarascon, *Science* **2011**, *334*, 928–935.
[2] J. E. Halls, A. Hawthornthwaite, R. J. Hepworth, N. A. Roberts, K. J. Wright, Y. Zhou, S. J. Haswell, S. K. Haywood, S. M. Kelly, N. S. Lawrence, J. D. Wadhawan, *Energy Environ. Sci.* **2013**, *6*, 1026–1041.
[3] M. Skyllas-Kazacos, C. Menictas, T. Lim, in *Electricity transmission, distribution and storage systems*, Elsevier, **2013**, pp. 398–441.
[4] A. Z. Weber, M. M. Mench, J. P. Meyers, P. N. Ross, J. T. Gostick, Q. Liu, *J. Appl. Electrochem.* **2011**, *41*, 1137.
[5] M. Skyllas-Kazacos, M. Rychcik, R. G. Robins, A. Fane, M. Green, *J. Electrochem. Soc.* **1986**, *133*, 1057.
[6] B. Zakeri, S. Syri, *Renewable Sustainable Energy Rev.* **2015**, *42*, 569–596.
[7] K. J. Kim, M.-S. Park, Y.-J. Kim, J. H. Kim, S. X. Dou, M. SkyllasKazacos, *J. Mater. Chem. A* **2015**, *3*, 16913–16933.
[8] S. Roe, C. Menictas, M. Skyllas-Kazacos, *J. Electrochem. Soc.* **2016**, *163*, A5023–A5028.
[9] A. M. Pezeshki, J. T. Clement, G. M. Veith, T. A. Zawodzinski, M. M. Mench, *J. Power Sources* **2015**, *294*, 333–338.
[10] K. J. Kim, S.-W. Lee, T. Yim, J.-G. Kim, J. W. Choi, J. H. Kim, M.-S. Park, Y.-J. Kim, *Sci. Rep.* **2014**, *4*, 6906.
[11] L. Estevez, D. Reed, Z. Nie, A. M. Schwarz, M. I. Nandasiri, J. P. Kizewski, W. Wang, E. Thomsen, J. Liu, J.-G. Zhang, V. Sprenkle, B. Li, *ChemSusChem* **2016**, *9*, 1455–1461.
[12] H. Kaneko, K. Nozaki, Y. Wada, T. Aoki, A. Negishi, M. Kamimoto, *Electrochim. Acta* **1991**, *36*, 1191–1196.
[13] K. Percin, A. Rommerskirchen, R. Sengpiel, Y. Gendel, M. Wessling, *J. Power Sources* **2018**, *379*, 228–233.
[14] A. Rommerskirchen, Y. Gendel, M. Wessling, *Electrochem. Commun.* **2015**, *60*, 34–37.
[15] C. Dennison, M. Beidaghi, K. Hatzell, J. Campos, Y. Gogotsi, E. Kumbur, *J. Power Sources* **2014**, *247*, 489–496.
[16] T. J. Petek, N. C. Hoyt, R. F. Savinell, J. S. Wainright, *J. Power Sources* **2015**, *294*, 620–626.
[17] K. Hatzell, M. Boota, E. Kumbur, Y. Gogotsi, *J. Electrochem. Soc.* **2015**, *162*, A5007–A5012.
[18] N. C. Hoyt, E. Agar, E. A. Nagelli, R. Savinell, J. Wainright, *J. Electrochem. Soc.* **2018**, *165*, E439–E444.
[19] J. Lohaus, D. Rall, M. Kruse, V. Steinberger, M. Wessling, *Electrochem. Commun.* **2019**, *101*, 104–108.
[20] C. Dennison, Y. Gogotsi, E. Kumbur, *Phys. Chem. Chem. Phys.* **2014**, *16*, 18241–18252.
[21] J. Lölsberg, O. Starck, S. Stiefel, J. Hereijgers, T. Breugelmans, M. Wessling, *ChemElectroChem* **2017**, *4*, 3309–3313.
[22] C. Fritzmann, M. Hausmann, M. Wiese, M. Wessling, T. Melin, *J. Membr. Sci.* **2013**, *446*, 189–200.
[23] S. Armbruster, O. Cheong, J. Lölsberg, S. Popovic, S. Yüce, M. Wessling, *J. Membr. Sci.* **2018**, *554*, 156–163.
[24] A. Rommerskirchen, A. Kalde, C. J. Linnartz, L. Bongers, G. Linz, M. Wessling, *Carbon* **2019**, *145*, 507–520.
[25] M. Eisenberg, C. Tobias, C. Wilke, *J. Electrochem. Soc.* **1954**, *101*, 306–320.
[26] K. B. Hatzell, M. Boota, Y. Gogotsi, *Chem. Soc. Rev.* **2015**, *44*, 8664–8687.
[27] A. Golovnev, M. E. Suss, *J. Chem. Phys.* **2018**, *149*, 144904.
[28] C.-N. Sun, F. M. Delnick, D. Aaron, A. Papandrew, M. M. Mench, T. A. Zawodzinski, *ECS Electrochem. Lett.* **2013**, *2*, A43–A45.
[29] J. Ma, C. Zhang, F. Yang, X. Zhang, M. Suss, X. Huang, P. Liang, *Environ. Sci. Technol.* **2020**, *54, 2*, 1177–1185.
[30] N. Jäckel, D. Weingarth, M. Zeiger, M. Aslan, I. Grobelsek, V. Presser, *J. Power Sources* **2014**, *272*, 1122–1133.

Manuscript received: February 13, 2020
Revised manuscript received: March 27, 2020
Accepted manuscript online: April 14, 2020

© 2020 The Authors. Published by Wiley-VCH Verlag GmbH & Co. KGaA